Desalination and Water Treatment
www.deswater.com
doi: 10.5004/dwt.2018.22316

114 (2018) 19–30
May

Optimization on the operating conditions of PRO process: towards improved net power density

Hongliu Wang[a,b,c], Yue Wang[a,b,c,*], Dongya Ma[a,b,c], Qian Zhang[a,b,c], Shichang Xu[a,c,*]

[a]*Chemical Engineering Research Center, School of Chemical Engineering and Technology, Tianjin University, Tianjin 300072, China, Tel. +86 22 85356553; emails: tdwy75@tju.edu.cn (Y. Wang), xushichang@sina.com (S. Xu), wanghongliu_@tju.edu.cn (H. Wang), mdy@tju.edu.cn (D. Ma), qian727318045@ tju.edu.cn (Q. Zhang)*
[b]*State Key Laboratory of Chemical Engineering, Tianjin 300072, China*
[c]*Tianjin Key Laboratory of Membrane Science and Desalination Technology, Tianjin 300072, China*

Received 26 November 2017; Accepted 5 April 2018

ABSTRACT

In the pressure-retarded osmosis (PRO) process, the power density was dramatically influenced by the operating conditions including the applied hydraulic pressure difference (ΔP), the ratio of feed to draw flow rate (V_F/V_D), and the ratio of draw flow rate to membrane area (V_D/S_m). A theoretical model considering the non-ideal effects of concentration polarization, reverse salt flux, and pressure losses in draw side through the membrane module was developed to predict the water flux of the PRO, from which the power density and specific energy were predicted. The optimization of operating conditions was conducted by the theoretical model to meet the PRO process' predefined economic viability of about 5.00 W m^{-2} for the power density. Experimental verification of the theoretical model was carried out when the applied pressure is <10 bar, which is the maximum pressure resistance of the forward osmosis membrane in the paper. The resulted optimal operating conditions were ΔP of 17 bar, V_F/V_D of 0.8, and V_D/S_m of 47 L min^{-1} m^{-2} using seawater–river system, under which the theoretical power density was 5.13 W m^{-2}, higher than the benchmark of 5.00 W m^{-2}. The error between the experimental and theoretical results was <5%, which demonstrated the theoretical model is reliable.

Keywords: Pressure-retarded osmosis; Operating conditions; Net power density; Osmotic power

1. Introduction

Due to the depletion of fossil fuels and the challenge of climate change [1], renewable energy sources (e.g., solar, wind, and ocean) have received extensive attention in recent years [2,3]. Among the many energy sources, osmotic energy from natural salinity gradients has been an attractive option [4,5], which has been estimated to be 2.6 TW about 13% of the current world energy consumption [6]. In order to effectively convert osmotic energy into electricity [7], the pressure-retarded osmosis (PRO) process has been one of the most effective methods currently [8,9].

In the PRO process, the concentration difference between the feed solution (dilute salt solution) and the draw solution (concentrated salt solution) across a semi-permeable membrane generates the osmotic pressure difference, which drives the permeation of water from the feed side to draw side [10,11]. And a hydraulic pressure, which is lower than the osmotic pressure difference, is applied to the draw solution to retard the permeation of water across the membrane [12]. Fig. 1 illustrates the common osmosis power plant, in which the feed and draw solutions are first pretreated to minimize membrane fouling; then, the draw solution is pressurized by a pressure exchanger; and the expanding volume of draw solution is extracted by a hydro turbine to generate the power.

The concept of PRO was initially conceived in the 1970s [13], and there was a resurgence of research on PRO in the last decade. In 2009, Statkraft built up the first PRO prototype

* Corresponding author.

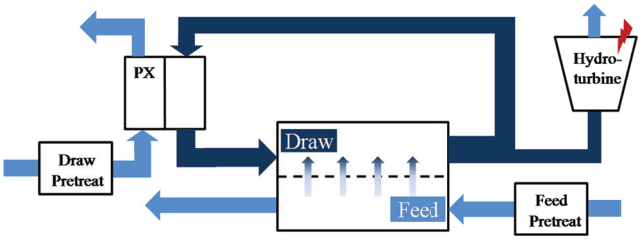

Fig. 1. A schematic diagram of a typically engineered PRO system.

in Norway [14]; the results showed that the power density was <1.5 W m^{-2}, which was undesirable, mainly due to the serious internal concentration polarization (ICP) in membrane's support layer. In consequence, the PRO prototype was deactivated in 2013. Through the test, Statkraft proposed that the minimum power density should achieve 5 W m^{-2} to make the system commercially working [15–17]. Membrane power density as the measure of the power generated over per unit membrane area is an important parameter of the system performance, due to the economical PRO system must have high power density.

The power density of the PRO system is depended on the osmotic pressure difference and the PRO membrane. Most PRO studies thus far have focused on PRO membranes, and there is tremendous progress in the development of PRO membranes. Hydration Technology Innovations (HTI) company first achieved batch production of cellulose triacetate flat sheet membranes and then produced thin film composite (TFC) membranes [18,19]. Until now, hollow fiber TFC membrane can withstand a hydraulic pressure of 23 bar and harvest membrane power density of 27 W m^{-2} when the draw and feed solutions are reverse osmosis (RO) seawater brine and deionized (DI) water, respectively [20]. However, due to the low pressure resistance of the commercialized PRO membrane, the draw solution concentration is limited. Using seawater–river water as draw–feed solutions is most common in the PRO progress, since the confluence of the river and the sea widely exists in nature. Although many literatures show that using seawater as draw solution is not the most efficient for PRO system, this research in the PRO process is still indispensable.

The PRO membrane performances differ intensely at separate operating condition; even further, the influence is not expressed as single variable oriented due to all the non-ideal effects together, like concentration polarization, reverse salt flux (RSF), and pressure losses [6,21]. Therefore, many models were established to study the optimal operating conditions, then to reduce the effects of the non-ideal factors, and to improve the membrane performance of the PRO system. He et al. [22] established a thermodynamic model to optimize the operational conditions, and then to maximize the power density and the extraction of energy from the PRO process. He et al. [23] also optimized the operating conditions and the membrane parameters of a scaled-up PRO process by maximizing the membrane power density and specific energy (SE). Touati and Tadeo [24] investigated the effect of the operating conditions on reverse salt diffusion and the produced power to reduce the influence of the non-ideal effects. In these works, only the theoretical model addressed the non-ideal effects to study the operating conditions. There is lack of specific experimental verification and optimization. And the parasitic pressure losses from friction in the membrane module need to be considered, which will outweigh the advantages of operating at high flow rates.

In this study, a theoretical model considering the non-ideal effects of external concentration polarization (ECP), ICP, RSF, and pressure loss in draw side through the membrane module was developed to predict the water flux, power density, and SE. Then, the operating conditions of the PRO process with seawater–river water as draw–feed solutions were optimized using the theoretical model. The operating conditions includes the applied hydraulic pressure (ΔP) on the draw solution, the ratio of feed to draw flow rate (V_F/V_D), and the ratio of flow rate to membrane area (V_D/S_m). And the theoretical model was verified by experiments when the ΔP is <10 bar, due to the poor pressure resistance of the forward osmosis (FO) membrane.

2. Theory

2.1. Concentration polarization

Concentration polarization refers to the non-liner concentration gradient across the membrane including ECP and ICP due to the accumulation of solute on the membrane surface and within the membrane support layer, respectively [25–27]. Due to the defect of the membrane, the effective concentration difference across the membrane ΔC_m is highly affected by concentration polarization and RSF as described in Eq. (1), where the draw solution faces the active layer, and the feed solution faces the support layer [24]:

$$\Delta C_m = \frac{C_{D,b}\exp\left(-\frac{J_W\delta_D}{D}\right) - C_{F,b}\exp\left(\frac{J_W\delta_F}{D}\right)\exp\left(\frac{J_W S}{D}\right)}{1+\frac{B}{J_W}\left[\exp\left(\frac{J_W\delta_F}{D}\right)\exp\left(\frac{J_W S}{D}\right) - \exp\left(-\frac{J_W\delta_D}{D}\right)\right]} \quad (1)$$

where B is the membrane's salt permeability; $C_{D,b}$ is the bulk draw concentration; $C_{F,b}$ is the bulk feed concentration, and δ is the boundary layer thickness, as shown in Eq. (2):

$$\delta = \frac{D}{k} \quad (2)$$

D is the salt diffusion coefficient, which is generally assumed to be constant, but in order to improve accuracy it can be calculated by C and T [4]:

$$D = 6.725\times10^{-6}\times\exp\left(1.546\times10^{-4}\times C - \frac{2513}{T}\right) \quad (3)$$

k is the mass transfer coefficient; it can be calculated by:

$$k = \frac{\mathrm{Sh}D}{\mathrm{dh}} \quad (4)$$

where Sh is the Sherwood number and is the hydraulic diameter. Sh is constituted by Reynolds number (Re), Schmidt

number (Sc), dh, and membrane thickness (L_s) in the following equations. However, Sh is different with various flow states.

$$\mathrm{Sh} = 1.85\left(\mathrm{ReSc}\,\mathrm{dh}/L_s\right)^{0.33}\left(\text{Laminar flow, Re} \le 2{,}000\right) \tag{5}$$

$$\mathrm{Sh} = 0.04\,\mathrm{Re}^{0.75}\mathrm{Sc}^{0.33}\,(\text{Turbulent flow, Re} > 2{,}000) \tag{6}$$

$$S = \frac{t\tau}{\varepsilon} \tag{7}$$

S is the structural parameter of the membrane support layer, as shown in Eq. (7) where t is the thickness; ε is the porosity; and τ is the tortuosity of the support layer.

2.2. Pressure loss of the membrane module

The pressure loss P_{loss} on draw side of the membrane by friction can be described by [4,6]:

$$5.99\times10^{-5}\times\Delta P^{-0.229} = \left(\frac{f*\rho*L*V^2}{4W^2P_{\text{loss}}}\right)^{1/3} \tag{8}$$

where ρ is density; V is the flow rate; L is the length of the membrane module; W is the width of the membrane module, is the dimensionless friction factor (Eq. (9)), and is constant:

$$f = \alpha_1\times\mathrm{Re}^{\alpha_2} \tag{9}$$

2.3. Water flux and reverse salt flux

The water flux (J_W) across the semi-permeable membrane is calculated by:

$$J_W = A(\Delta\pi - \Delta P) \tag{10}$$

where A is the water permeability coefficient of the membrane; Δπ and ΔP are the trans-membrane osmosis pressure and applied hydraulic pressure on the draw side, respectively. Osmotic pressure is a function of temperature and concentration [4].

The water flux (J_W) considering the non-ideal effects of concentration polarization, RSF, and pressure losses on the draw side of the membrane module is presented by:

$$J_W = A\left\{\frac{\pi_{D,b}\exp\left(-\frac{J_W}{k_D}\right)-\pi_{F,b}\exp\left(\frac{J_W}{k_F}\right)\exp\left(J_WK\right)}{1+\frac{B}{J_W}\left[\exp\left(\frac{J_W}{k_F}\right)\exp\left(J_WK\right)-\exp\left(-\frac{J_W}{k_D}\right)\right]}-\Delta P+P_{\text{loss}}\right\} \tag{11}$$

However, salt permeate is in the opposite direction with water across the membrane. The RSF (J_s) is calculated by:

$$J_s = B\Delta C \tag{12}$$

where B is the salt permeability coefficient of the membrane, and ΔC is the concentration difference across the membrane. To improve water flux, many efforts have been made to optimize the trade-off between water permeability A and salt permeability B of the membrane [6].

The water flux across the membrane is influenced by the non-ideal effects, which include pressure losses and concentration polarization. In our previous publication, the detailed description of concentration polarization has been presented in [21].

2.4. Power density

Power of the PRO process is determined by the expanding volume of high-pressure draw solution. The power density (W') is the obtained power per unit membrane area, and it is the product of water flux and applied hydraulic pressure in the draw solution. It can be calculated by dividing system energy output ($\Delta P\Delta V$), by the membrane area (S_m), as described in Eq. (13) [24]:

$$W = \frac{\Delta P\Delta V}{S_m} \tag{13}$$

$$\Delta V = J_WS_m \tag{14}$$

where ΔV is the permeate flow rate. The peak power density is achieved when $\Delta P = \Delta\pi/2$, which means that only half of the salinity gradient can be transformed to power.

2.5. Specific energy

The SE quantifies the extracted energy per unit volume of feed (V_F) and draw (V_D) solutions. It is calculated by dividing the energy output ($\Delta P\Delta V$), by the sum of the feed flow rate (V_F), and draw flow rate (V_D):

$$\mathrm{SE} = \frac{\Delta P\Delta V}{V_F+V_D} \tag{15}$$

With a given solution pairing, the extracted maximum SE can be seen as the volumetric energy density. SE is an important concept to quantify system performance because the amount of solution volume determines the energetic costs of the system, such as pretreatment and pumping.

2.6. Net power density

The efficiencies of the mechanical and electrical devices including the pumps, hydro turbine, generator, and energy recovery device (ERD) in the PRO process cannot reach 100% due to energy losses. Energy loss of ERD is supplemented by feed, draw, and booster pumps. In addition, the frictional losses in piping, valves, and PRO membrane modules are also provided by the pump, which can degrade the performance of PRO process. The power consumption of the pump is calculated by Eq. (16). And the total power consumption of all pumps is calculated by Eq. (17):

$$W_{\text{pump}} = \Delta P_{\text{pump}}\times V_{\text{pump}}\times\frac{1}{\eta_{\text{pump}}} \tag{16}$$

$$\Sigma W_{pump} = W_{FP} + W_{DP} + W_{booster\ pump} \quad (17)$$

where η_{pump} in Eq. (16) is the efficiency of the pump. W_{FP} and W_{DP} in Eq. (17) are the power consumption of feed and draw solutions, respectively.

The power generation by the hydro turbine is calculated by Eq. (18):

$$W_{turbine} = \Delta P_{turbine} \times V_{turbine} \times \eta_{turbine} \times \eta_{generator} \quad (18)$$

where $\eta_{turbine}$ and $\eta_{generator}$ are the efficiencies of turbine and generator, respectively. When the power generation by the hydro turbine (gross power) is larger than the power consumption of pumps, the PRO process is feasible. The net power is given by the following equation:

$$W_{net} = W_{turbine} - \sum W_{pump} \quad (19)$$

The net power density is calculated by dividing the net power, W_{net}, by the membrane area S_m:

$$W'_{net} = \frac{W_{turbine} - \sum W_{pump}}{S_m} \quad (20)$$

3. Research methodology

3.1. Modeling of PRO

The optimum operating conditions, including the applied hydraulic pressure difference (ΔP) and flow rates of feed (V_F) and draw (V_D) solutions, were determined by the theoretical analysis and experiments to improve the output power according to the procedure illustrated in Fig. 2. First, the optimal hydraulic pressure difference (ΔP_{opt}) was obtained by maximizing the water flux (J_W) and power density (W') of the membrane module. Next, V_F/V_D and V_D/S_m (L min^{-1} m^{-2}) were determined by the theoretical calculation to balance the power density (W') and SE of the membrane module. Afterward, the calculated V_F/V_D and V_D/S_m were further optimized by the theoretical model. Then, the optimal feed and draw flow rates of the module were achieved by the selected membrane area.

Finally, the optimal operating conditions including ΔP_{opt}, V_F, and V_D were applied to the PRO system shown as Fig. 1 to calculate ΔV (Eq. (4)) and the net power density. The flow rates were used for calculating the power consumption of the pumps, and the efficiencies of the equipment were shown in Table 1 [28].

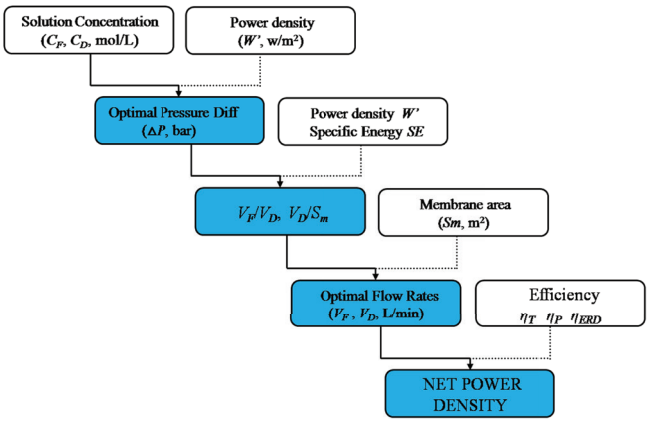

Fig. 2. Logic framework for determining the optimal pressure difference, the ratio of feed to draw flow rate, and feed and draw flow rates to calculate net power.

3.2. Experimental setup

Membranes were tested in a custom four-port rectangular cell with length L = 250 mm, width w = 84 mm, and channel height h = 4 mm. Fig. 3 showed the custom cell assembly. Commercial FO membrane was the flat sheet TFC membrane from CSM (Korea). The solutions were obtained by incorporating chemical-grade sodium chloride (NaCl) into DI water, and the concentrations were measured by a conductivity meter. Two solutions were supplied to the membrane cell from solution tank via pumps. Feed flow rates were set by adjusting the speed of peristaltic pump. Draw flow rates were controlled by flow meter, and the hydraulic pressure in the cell was regulated via a bypass valve. Mass change of feed solution over time was recorded using an electronic balance.

3.3. Membrane characterization

The evaluation of apparent membrane performance parameters using PRO method under varying draw pressures was proposed by [27]. In this study, a new PRO method was used to determine water permeability A, salt permeability B, and structure parameter S of the membrane. The test conditions are shown in Table 2.

Table 1
The efficiencies of the equipment in the PRO process

Equipment	Efficiency (%)
Draw pump	80
Booster pump	80
Feed pump	80
ERD	95
Hydro turbine	87
Generator	98

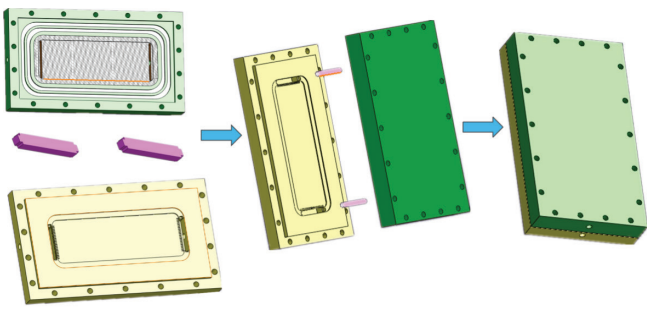

Fig. 3. The SolidWorks figure of membrane cell.

Table 2
Conditions for membrane characterization tests

	Water permeability	Salt permeability	Structure parameter
Testing platform	PRO test	PRO test	FO test
Temperature	20°C	20°C	20°C
Feed concentration, $C_{F,b}$	0 mol L^{-1}	0.04 mol L^{-1}	0 mol L^{-1}
Feed flow rate, V_F	1.2 L min^{-1}	1.2 L min^{-1}	1.2 L min^{-1}
Feed velocity, u_F	0.25 m s^{-1}	0.25 m s^{-1}	0.25 m s^{-1}
Draw concentration $C_{D,b}$	0 mol L^{-1}	0 mol L^{-1}	1 mol L^{-1}
Draw flow rate, V_D	1.2 L min^{-1}	1.2 L min^{-1}	1.2 L min^{-1}
Draw velocity, u_D	0.25 m s^{-1}	0.25 m s^{-1}	0.25 m s^{-1}
Hydraulic pressure, ΔP	8, 6, 4, 2 bar	8, 5, 3 bar	0 bar

In all cases, the membrane orientation was the active layer facing toward the draw solution and the support layer facing toward the feed solution. And all the tests were last for over 60 min to ensure that the system was steady before collecting data. In order to obtain accurate membrane parameters, all the tests were repeated at least 5 times with solution temperatures were stabilized at 20°C ± 0.5°C. Flow rates were set as 1.2 L min^{-1} at the membrane inlet, and the corresponding inlet flow velocities were set as 0.25 m s^{-1}, which is the recommended value in PRO process.

3.3.1. Water permeability coefficient of the membrane

In order to improve the accuracy of the membrane parameters, the water permeability coefficient (A) was tested by using PRO method, which is similar to the RO method. The water permeability coefficient was calculated by following equations [29]:

$$J_W = \frac{\Delta V}{S_m} \tag{21}$$

$$A = \frac{J_W}{\Delta P} \tag{22}$$

where ΔV is permeate flow rate, L min^{-1}.

At each stage, water flux was calculated by the changes of mass and conductivity in feed and draw solutions. In the process, the feed and draw solutions were DI water. At the first stage, water flux (J_{W1}) was measured at hydraulic pressure of 8 bar until the permeate flow rate remained stable. At the end of this stage, the hydraulic pressure difference was reduced by 2 bar to get the desired value. The resulting reduced water flux (J_{W2}) was measured. The third and fourth stages were performed in the same way until ΔP = 2 bar.

3.3.2. Salt permeability coefficient of the membrane

The salt permeability coefficient (B) was also tested using PRO method. The salt permeability coefficient was calculated by Eq. (23):

$$B = J_W \left(\frac{1-R}{R}\right) \exp\left(-\frac{J_W}{k}\right) \tag{23}$$

where k is the mass transfer coefficient; R is the salt rejection rate, which was calculated by Eq. (24).

$$R = 1 - \frac{C_P}{C_F} \tag{24}$$

where C_P is the concentration of the permeate solution; C_F is the concentration of the feed solution. Water flux was measured using the feed solution of 0.04 M NaCl and permeate solution of DI water; at each stage, the permeate concentration was measured by a conductivity meter. At the first stage, hydraulic pressure difference (ΔP = 3 bar) was applied to the draw side for 60 min. The permeate volume $V_{C,i}$ and concentration $C_{C,i}$ became change and completed the measurement at predetermined time intervals. The permeate concentration was calculated by Eqs. (25) and (26). The second and third stages were performed in the same way at hydraulic pressure difference ΔP = 5 and 8 bar, respectively.

$$C_P = \frac{M_{\mathrm{PS}}}{V_{\mathrm{C},\,i+1}} \tag{25}$$

$$C_{C,i} V_{C,i} + M_{\mathrm{PS}} = C_{C,i+1}(V_{C,i} + V_{C,i+1}) \tag{26}$$

where M_{PS} is the mass of the permeate salt.

3.3.3. Structure parameter of membrane

A FO test was also examined to determine the membrane's structure parameter S. The concentrations of the feed and draw solutions were 0 and 1 mol L^{-1}, respectively. The outlet concentrations of the feed and draw solutions C_F and C_D were measured using conductivity meters. The structure parameter S was calculated by the following equation:

$$S = \frac{D}{J_W} \ln\left(\frac{B + A \cdot \pi_{D,b}}{B + J_W + A \cdot \pi_{F,m}}\right) \tag{27}$$

where $\pi_{D,b}$ and $\pi_{F,m}$ are the osmotic pressure of the bulk draw and feed solutions at the membrane surface, respectively. There is a hypothesis in this equation: $\pi_{F,m} = \pi_{F,b}$. It was mainly due to the fact that $C_{F,m}$ is not possible to measure directly.

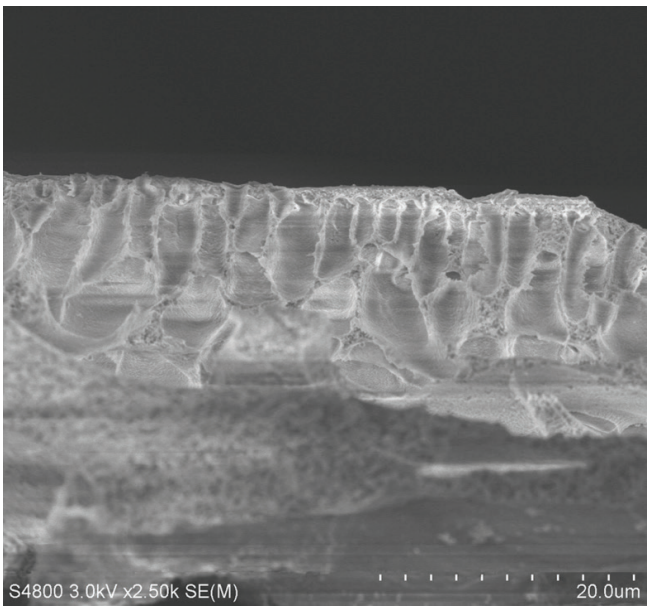

Fig. 4. The cross-sectional SEM image of the flat sheet FO membrane.

4. Results and discussions

4.1. Parameters of the membrane

In this paper, the characterization can be quantitatively described as water permeability coefficient A =1.53 LMH bar^{-1}, salt permeability coefficient B =1.63 LMH, structure parameter S = 747.33 μm and be observed through cross-sectional SEM in Fig. 4.

4.2. Theoretical and experimental optimization on operating conditions of PRO process

4.2.1. Theoretical and experimental optimization on operating conditions of PRO process at different ratios of feed to draw flow rate

In PRO process, power density (W') and SE are important parameters to evaluate the feasibility of the PRO process, which are expressed by the operating conditions ΔP, V_F/V_D, and V_D/S_m (Eqs. (3) and (5)) by considering concentration polarization and pressure loss in the membrane module. Figs. 5 and 6 illustrate the theoretical results of W' and SE at fixed V_F/V_D ratio of 0.6, 0.8, 1.0 and the V_D/S_m ratio in between 25 and 300. In Fig. 5, an increment in V_D/S_m clearly increases

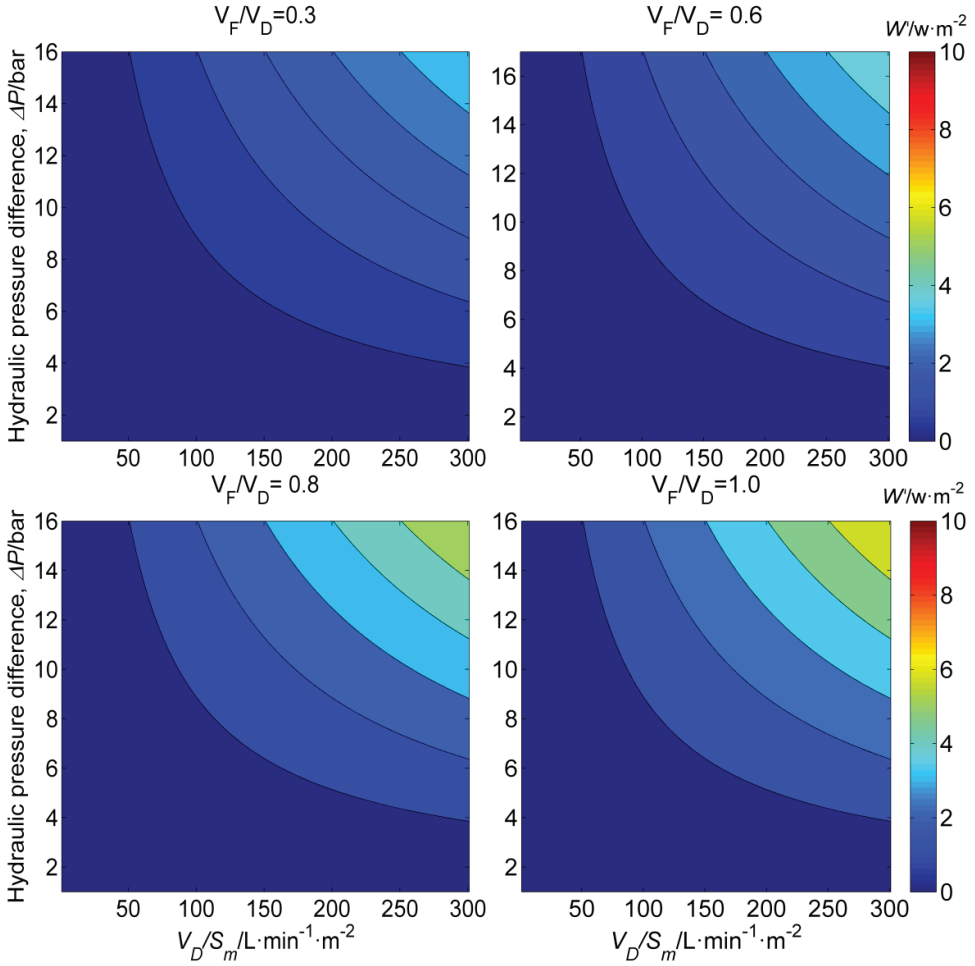

Fig. 5. The power density as functions of ΔP and V_D/S_m at V_F/V_D = 0.3, 0.6, 0.8, 1.0, respectively.

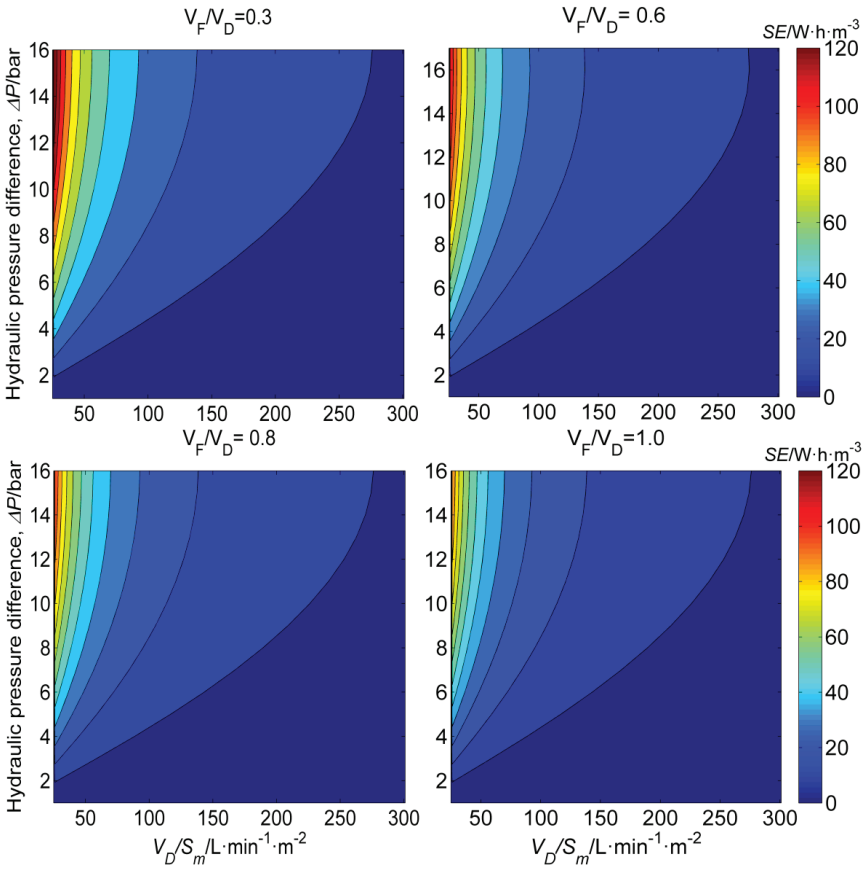

Fig. 6. The SE as functions of ΔP and V_D/S_m at V_F/V_D = 0.6, 0.8, 1.0, respectively.

the power density at a fixed hydraulic pressure difference, and the power density reaches its maximum at the hydraulic pressure difference around 15–16 bar that is a little larger than $\Delta\pi/2$, due to the pressure loss on the draw side. Similar trends are found when the V_F/V_D ratios are 0.8 and 1.0. When the values of V_F/V_D increase from 0.3 to 1.0, the power density gradually increases. However, the power density slightly increases at V_F/V_D from 0.8 to 1.0; it is due to the fact that when V_F/V_D = 0.8, the permeation process is close to stable.

The variation of SE as functions of ΔP and V_D/S_m is illustrated in Fig. 6. Interestingly, the SE also reaches its maximum at the hydraulic pressure difference of around 15–16 bar. It also can be seen that an increment in V_F/V_D clearly decreases the SE at low V_D/S_m ratios, and ΔP shows limited impacts on both power density and SE. This can be ascribed to the dramatic variation of the draw and feed solutions' concentration along the membrane with the water penetration across the membrane. At high V_D/S_m ratios, ΔP becomes more influential since the changes of solution concentrations, which are induced by water permeation, are not so evident. Therefore, the relatively low flow rates are beneficial for the equilibrium of the power density and SE. And the optimum operating conditions are V_F/V_D = 0.8 and V_D/S_m < 100 L min^{-1} m^{-2} when uses seawater–river water as draw–feed solutions.

The theoretical ranges of the PRO process are further optimized by the PRO performance of water flux, power density, and the net power density. And the results are verified by experiments, which were repeated three times at different hydraulic pressure differences (ΔP = 0, 2, 4, 6, 8, and 10 bar), due to the flat sheet FO membrane used in the experiments can withstand a maximum pressure differential of 10 bar that limits the ability to conduct experiments at high pressure, and the experimental conditions are summarized in Table 3. Fig. 7 illustrates the theoretical and experimental results. The error between the two results is <5%, which proves the accuracy of the theoretical model. Fig. 7 shows that the optimum applied

Table 3
Conditions for testing membrane performance at different V_F/V_D ratios

Description	Test conditions
Temperature	20°C
Feed concentration, $C_{F,b}$	0.05 mol L^{-1}
Feed flow rate, V_F	0.48, 0.64, 0.8 L min^{-1}
Feed velocity, u_F	0.10, 0.14, 0.17 m s^{-1}
Draw concentration, $C_{D,b}$	0.6 mol L^{-1}
Draw flow rate, V_D	0.8 L min^{-1}
Draw velocity, u_D	0.17 m s^{-1}
Hydraulic pressure difference, ΔP	2, 4, 6, 8, 10 bar
Test length	60 min
Membrane orientation	Active layer facing draw

hydraulic pressure differences are same at different feed flow rates, because the pressure losses on the feed side are not taken into account. RSF is higher than those obtained from flat sheet FO membrane (HTI company), since the higher salt permeability coefficient of the membrane used in this study. As V_F/V_D increases from 0.6 to 1.0, water flux increases from 13.20 to 13.36 L m^{-2} h^{-1}; power density increases from 4.66 to 4.71 W m^{-2}; and the pressure loss is 2.30 bar (Fig. 8) at the peak power point, 16 bar. However, with the increase of V_F/V_D from 0.8 to 1.0, the power density only increases 0.02 W m^{-2} that cannot offset the increment of energy consumption of pumps, due to the effects of parasitic pressure losses in draw side, which are proportional to flow rates. Therefore, the ratio of feed to draw flow rate V_F/V_D = 0.8 contributes to improve the net power of the PRO system, which is identical with the theoretical result in the previous section.

4.2.2. Theoretical and experimental optimization on operating conditions of PRO process at different feed and draw flow rates

To further optimize the operating conditions, water flux (J_W), power density (W'), RSF (J_s), and net power density(W_{net}) are studied at ΔP = 0, 2, 4, 6, 8, and 10 bar, and higher pressure points are also calculated by the theoretical model. The conditions used in this section are summarized in Table 4. The experimental and theoretical results are showed in Fig. 9.

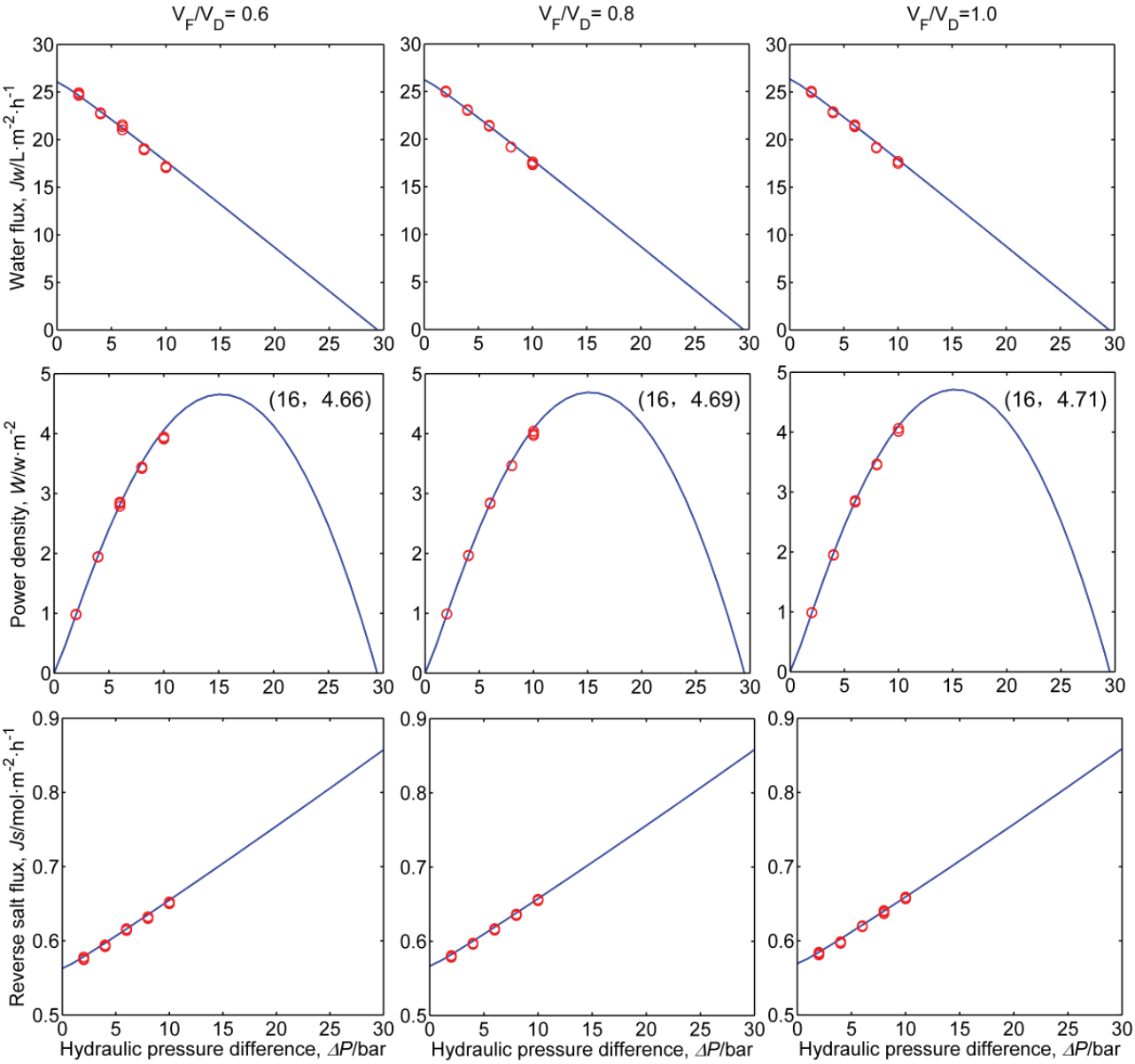

Fig. 7. PRO performance when T = 20°C, $C_{F,b}$ = 0.05 mol L^{-1}, and $C_{D,b}$ = 0.6 mol L^{-1}. Experimental results (red points) and theoretical results (blue lines) are shown for water permeate flux (J_W), power density (W'), and RSF (J_s), as functions of hydraulic pressure difference ΔP at V_F/V_D = 0.6, 0.8, 1.0, respectively. And the draw flow rates are fixed at 0.8 L min^{-1}.

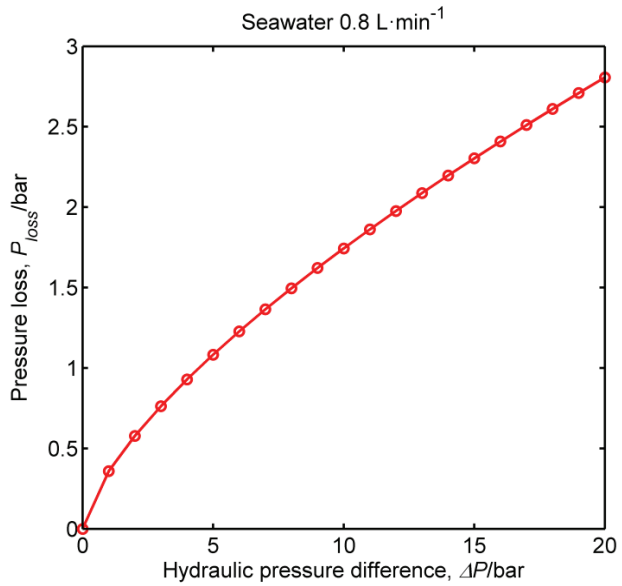

Fig. 8. The draw side pressure loss P_{loss} as functions of hydraulic pressure difference ΔP at draw flow rate V_D = 0.8 L min^{-1}.

Table 4
Conditions for testing membrane performance at different draw and feed flow rates

Description	Test conditions
Temperature	20°C
Feed concentration, $C_{F,b}$	0.05 mol L^{-1}
Feed flow rate, V_F	0.64, 0.8, 1.0 L min^{-1}
Feed velocity, u_F	0.14, 0.17, 0.21 m s^{-1}
Draw concentration, $C_{D,b}$	0.6 mol L^{-1}
Draw flow rate, V_D	0.8, 1.0, 1.25 L min^{-1}
Draw velocity, u_D	0.17, 0.20, 0.27 m s^{-1}
Hydraulic pressure difference, ΔP	2, 4, 6, 8, 10 bar
Test length	60 min
Membrane orientation	Active layer facing draw

RSF increases with the pressure increases applied in draw side, which is harmful to the membrane performance, that is, plug the membrane support layer and reduce the effective driving force. As V_D increases from 0.8 to 1.25 L min^{-1}, water flux increases from 13.30 to 15.66 L m^{-2} h^{-1}, and power density increases from 4.69 to 5.37 W m^{-2} at the respective peak power point. The optimal ΔP increases from 17 to 20 bar as the draw flow rate increases from 0.8 to 1.25 L min^{-1}, it is due to the fact that the draw side pressure loss increases from 2.30 to 5.91 bar at ΔP = 16 bar (Fig. 10). The power that is required to supply these parasitic loads will cause the decrement of the net power density. When the flow rates V_F is 0.8 L min^{-1} and V_D is 1.0 L min^{-1}, the power density W' is 5.13 W m^{-2} at the peak power point (17 bar), which is higher than the minimum power density 5 W m^{-2}. The net power density is positive when the draw flow rate ≤ 1.0 L min^{-1}. And when the draw flow rates are between 0.64 and 0.8 L min^{-1}, there is a modest increase in net power density, from 0.48 to 0.77 W m^{-2}. In fact, when the draw flow rate is beyond 1.0 L min^{-1}, the net power density begins declining. Hence, the optimum draw flow rate is selected as 1.0 L min^{-1} at which the net power density is the largest with the membrane area of 0.021 m^2 of the PRO system.

5. Conclusions

Optimizations on the operating conditions of the PRO process for seawater–river system were carried out in this paper. A theoretical model of the water flux was developed considering the non-ideal effects of concentration polarizations, RSF, and pressure losses in draw side through the membrane module. Validation experiments of the theoretical model were also implemented under the applied pressure of <10 bar. The conclusions are as follows:

- For the theoretical model, the optimal operating conditions of seawater–river system were the ΔP of around 17 bar, the V_F/V_D ratio of 0.8, and V_D/S_m ratio of 47 L m^{-2} min^{-1}, under which the power density could reach up to 5.13 W m^{-2} above the benchmark of 5.00 W m^{-2}.
- The experimental results of both the water flux and the power density of the PRO process were in a good agreement with the theoretical results under the applied pressure of <10 bar. The error is less than 5%, indicating that the theoretical models are reliable.

Symbols

A	—	Water permeability, L m^{-2} h^{-1} bar^{-1}
B	—	Solute permeability, L m^{-2} h^{-1}
S	—	Structure parameter, μm
J_W	—	Water flux, L m^{-2} h^{-1}
ΔP	—	Hydraulic pressure difference, bar
J_s	—	Reverse salt flux, mol m^{-2} h^{-1}
ΔC	—	Concentration difference across the membrane, mol L^{-1}
W'	—	Power density, W m^{-2}
ΔV	—	Permeate flow rate, L min^{-1}
S_m	—	Membrane area, m^2
SE	—	Specific energy, W m^{-2}
V_F	—	Feed flow rate, L min^{-1}
V_D	—	Draw flow rate, L min^{-1}
W_{pump}	—	Power consumption of the pump, W
η_{pump}	—	Pump efficiency, %
$W_{turbine}$	—	Power generation by the hydro turbine, W
$\eta_{turbine}$	—	Turbine efficiency, %
$\eta_{generator}$	—	Generator efficiency, %
W_{net}	—	Net power density, W m^{-2}
D	—	Bulk diffusion coefficient, m^2 s^{-1}
δ	—	Boundary layer thickness, m
k	—	Mass transfer coefficient, m s^{-1}
Sh	—	Sherwood number
dh	—	Hydraulic diameter of the flow channel, m
Sc	—	Schmidt number
L_s	—	Membrane thickness, m
Re	—	Reynolds number
t	—	Porous support layer thickness, m

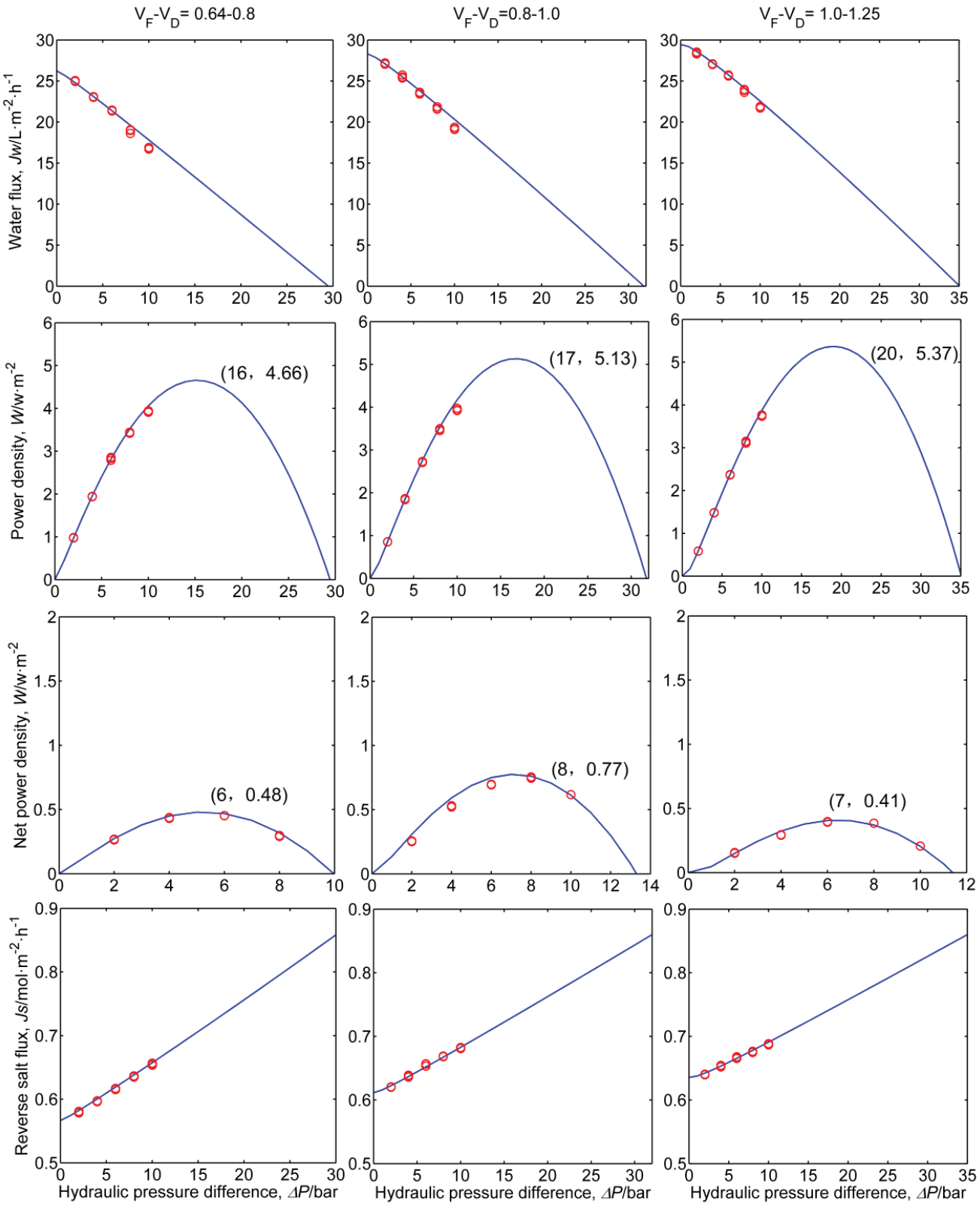

Fig. 9. PRO performance when T = 20°C, $C_{F,b}$ = 0.05 mol L^{-1}, and $C_{D,b}$ = 0.6 mol L^{-1}. Experimental results (red points) and theoretical results (blue lines) are shown for water permeate flux (J_W), power density (W'), RSF (J_s), and the net membrane power density (W_{net}) as functions of hydraulic pressure difference ΔP at V_F/V_D = 0.8, respectively.

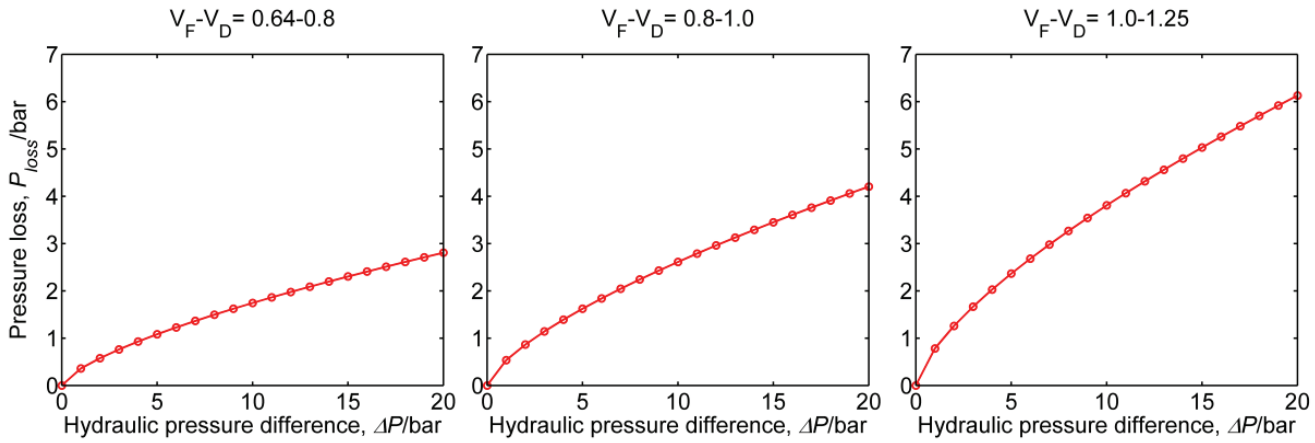

Fig. 10. The draw side pressure loss P_{loss} as functions of hydraulic pressure difference ΔP at different ratios of feed to draw flow rate.

ε	—	Porous support layer porosity, m
τ	—	Porous support layer tortuosity
K	—	Solute resistivity for diffusion within the porous support layer, s m^{-1}
R	—	Universal gas constant, Nm mol^{-1} K^{-1}
T	—	Absolute temperature, K
P_{loss}	—	Pressure loss, bar
L	—	The length of the membrane module, m
W	—	The width of the membrane module, m
f	—	The dimensionless friction factor
M_{PS}	—	The mass of the permeate salt

Greek

π	—	Osmotic pressure, bar
ρ	—	Density, kg m^{-3}

Subscripts

D	—	Draw
F	—	Feed
m	—	Membrane
s	—	Salt
w	—	Water
P	—	Permeate

Acknowledgment

This research is supported by the National Key R&D Program of China (2017YFC0403800).

References

[1] S. Lin, A.P. Straub, M. Elimelech, Thermodynamic limits of extractable energy by pressure retarded osmosis, Energy Environ. Sci., 7 (2014) 2706–2714.
[2] S. Zhang, T.-S. Chung, Osmotic power production from seawater brine by hollow fiber membrane modules: net power output and optimum operating conditions, AIChE J., 62 (2016) 1216–1225.
[3] H. Sharifan, H.T. Madsen, A. Morse, High performance in power generation by pressure-retarded osmosis (PRO) from hypersalinity gradient: case study of hypersaline Lake of Urmia, Iran, Desal. Wat. Treat., 71 (2017) 302–311.
[4] F. La Mantia, M. Pasta, H.D. Deshazer, B.E. Logan, Y. Cui, Batteries for efficient energy extraction from a water salinity difference, Nano Lett., 11 (2011) 1810–1813.
[5] J.C. da Silva, C.P. Borges, Development and analysis of membranes for osmotic processes, Desal. Wat. Treat., 70 (2017) 24–33.
[6] J. Maisonneuve, P. Pillay, C.B. Laflamme, Pressure-retarded osmotic power system model considering non-ideal effects, Renew. Energy, 75 (2015) 416–424.
[7] J. Maisonneuve, C.B. Laflamme, P. Pillay, Experimental investigation of pressure retarded osmosis for renewable energy conversion: towards increased net power, Appl. Energy, 164 (2016) 425–435.
[8] B.E. Logan, M. Elimelech, Membrane-based processes for sustainable power generation using water, Nature, 488 (2012) 313–319.
[9] F. Helfer, C. Lemckert, Y.G. Anissimov, Osmotic power with pressure retarded osmosis: theory, performance and trends – a review, J. Membr. Sci., 453 (2014) 337–358.
[10] A. Altaee, G. Zaragoza, A. Sharif, Pressure retarded osmosis for power generation and seawater desalination: performance analysis, Desalination, 344 (2014) 108–115.
[11] Y. Choi, S. Vigneswaran, S. Lee, Evaluation of fouling potential and power density in pressure retarded osmosis (PRO) by fouling index, Desalination, 389 (2016) 215–223.
[12] N.Y. Yip, M. Elimelech, Thermodynamic and energy efficiency analysis of power generation from natural salinity gradients by pressure retarded osmosis, Environ. Sci. Technol., 46 (2012) 5230–5239.
[13] A.P. Straub, A. Deshmukh, M. Elimelech, Pressure-retarded osmosis for power generation from salinity gradients: is it viable? Energy Environ. Sci., 9 (2016) 31–48.
[14] R.J. Aaberg, Osmotic power: a new and powerful renewable energy source? Refocus, 4 (2003) 48–50.
[15] S.E. Skilhagen, J.E. Dugstad, R.J. Aaberg, Osmotic power — power production based on the osmotic pressure difference between waters with varying salt gradients, Desalination, 220 (2008) 476–482.
[16] K. Gerstandt, K.V. Peinemann, S.E. Skilhagen, T. Thorsen, T. Holt, Membrane processes in energy supply for an osmotic power plant, Desalination, 224 (2008) 64–70.
[17] T. Thorsen, T. Holt, The potential for power production from salinity gradients by pressure retarded osmosis, J. Membr. Sci., 335 (2009) 103–110.
[18] J.R. McCutcheon, M. Elimelech, Modeling water flux in forward osmosis: implications for improved membrane design, AIChE J., 53 (2007) 1736–1744.

[19] A.P. Straub, N.Y. Yip, M. Elimelech, Raising the bar: increased hydraulic pressure allows unprecedented high power densities in pressure-retarded osmosis, Environ. Sci. Technol. Lett., 1 (2014) 55–59.
[20] C.F. Wan, T.-S. Chung, Osmotic power generation by pressure retarded osmosis using seawater brine as the draw solution and wastewater retentate as the feed, J. Membr. Sci., 479 (2015) 148–158.
[21] S. Xu, Y. Liu, Y. Wang, M. Zhang, Q. Xiao, Y. Duan, Influential analysis of concentration polarization on water flux and power density in PRO process: modeling and experiments, Desalination, 412 (2017) 39–48.
[22] W. He, Y. Wang, M.H. Shaheed. Energy and thermodynamic analysis of power generation using a natural salinity gradient based pressure retarded osmosis process, Desalination, 350 (2014) 86–94.
[23] W. He, Y. Wang, L.M. Mujtaba, M.H. Shaheed, An evaluation of membrane properties and process characteristics of a scaled-up pressure retarded osmosis (PRO) process, Desalination, 378 (2016) 1–13.
[24] K. Touati, F. Tadeo, Study of the reverse salt diffusion in pressure retarded osmosis: influence on concentration polarization and effect of the operating conditions, Desalination, 389 (2016) 171–186.
[25] G.D. Mehta, S. Loeb, Internal polarization in the porous substructure of a semi permeable membrane under pressure-retarded osmosis, J. Membr. Sci., 4 (1978) 261–265.
[26] Y. Wang, M. Zhang, Y. Liu, Q. Xiao, S. Xu, Quantitative evaluation of concentration polarization under different operating conditions for forward osmosis process, Desalination, 398 (2016) 106–113.
[27] J. Kim, B. Kim, D. Inhyuk Kim, S. Hong, Evaluation of apparent membrane performance parameters in pressure retarded osmosis processes under varying draw pressures and with draw solutions containing organics, J. Membr. Sci., 493 (2015) 636–644.
[28] S. Loeb, Large-scale power production by pressure-retarded osmosis, using river water and sea water passing through spiral modules, Desalination, 143 (2002) 115–122.
[29] G. Blandin, D.T. Myat, A.R.D. Verliefde, P. Le-Clech, Pressure assisted osmosis using nanofiltration membranes (PAO-NF): towards higher efficiency osmotic processes, J. Membr. Sci., 533 (2017) 250–260.